Ultracold Bose Gases in Dynamic Disorder with Tunable Correlation Time

Benjamin Nagler, Martin Will, Silvia Hiebel, Sian Barbosa, Jennifer Koch, Michael Fleischhauer, and Artur Widera*
Department of Physics and Research Center OPTIMAS, Technische Universität Kaiserslautern, 67663 Kaiserslautern, Germany

(Received 17 August 2020; revised 25 December 2021; accepted 4 May 2022; published 6 June 2022)

We study experimentally the dissipative dynamics of ultracold bosonic gases in a dynamic disorder potential with tunable correlation time. First, we measure the heating rate of thermal clouds exposed to the dynamic potential and present a model of the heating process, revealing the microscopic origin of dissipation from a thermal, trapped cloud of bosons. Second, for Bose-Einstein condensates, we measure the particle loss rate induced by the dynamic environment. Depending on the correlation time, the losses are either dominated by heating of residual thermal particles or the creation of excitations in the superfluid, a notion we substantiate with a rate model. Our results illuminate the interplay between superfluidity and time-dependent disorder and on more general grounds establish ultracold atoms as a platform for studying spatiotemporal noise and time-dependent disorder.

DOI: 10.1103/PhysRevLett.128.233601

Disorder is ubiquitous, and its impact on physical systems has been studied intensely in recent decades [1,2]. Most investigations were focused on static disorder, in which single-particle wave transport can be suppressed due to Anderson localization [3–8], and thermalization is absent in certain interacting systems [7–11]. Since phenomena like Anderson localization are based on interference, modulating disorder in time has dramatic effects. Recent studies of dynamic disorder in classical and quantum systems focusing on transport showed, in stark contrast to the static case, that it can be supported [12,13] and even accelerated beyond the ballistic regime [14,15]. However, the interplay between superfluidity and long-range coherence with time-dependent disorder, and dissipation induced by the dynamic environment, have not yet been investigated in experiments. The impact of dynamic disorder is of broad interest, for example, in the context of energy transfer in biological systems [16,17], the electrical conductivity of ionic polymers [18] and microemulsions [19], chemical reactions [20], wave propagation in the sea [21], superconductors [22], and quantum walks [23]. Theoretical works on spatiotemporal noise predict a nonequilibrium phase transition [24,25] which is induced by the random environment. For quantum systems, it seems natural to pose the question if there is an extention of preparing nonequilibrium states by spatiotemporal periodic drive [26,27] to the case of general broadband spatiotemporal noise. This novel regime is particularly complicated by the nonlinearity of interacting quantum systems as Bose-Einstein condensates (BECs), giving rise to collective phenomena such as superfluid flow. One potential challenge is the unfavorable heating of atomic systems due to energy absorption from the dynamic environment [26]. The role of dissipation is of general interest in the paradigm of open quantum systems [28], which is realized by, e.g., quantum gases coupled to environments with spatiotemporal noise.

Here, we study the nonequilibrium dynamics of ultracold molecular Li_2 gases in tunable dynamical disorder. We employ a novel scheme to realize a time-dependent optical speckle potential with variable correlation time, inspired by a method for the decorrelation of light fields [29]. For ultracold, thermal ensembles, we observe the microscopic onset of dissipation for decreasing correlation time, which is well described by a random-walk model in momentum space. For BECs, the disorder additionally creates direct excitations in the superfluid, depleting the superfluid fraction. We model the dissipative dynamics of the quantum gas by an open-system rate model, treating the superfluid excitations in two complementary ways. Importantly, comparison with experimental data suggests a window of correlation times having negligible superfluid excitations, well suited for studies of nonequilibrium dynamics of quantum fluids.

Experimentally, we prepare dilute gases of bosonic $^6Li_2$ Feshbach molecules in a cigar-shaped hybrid magnetic-optical trap [Fig. 1(a)]; for details see Refs. [30,31]. The magnetic field close to a magnetic Feshbach resonance at 832.2 G [32] sets the s-wave scattering length a between the molecules and thus their binding energy. Typical thermal (degenerate) samples contain $> 10^5$ molecules at a temperature of $T = 590$ nK (50 nK). A repulsive optical speckle potential [33] at a wavelength of 532 nm introduces the disorder. The typical size of the anisotropic speckle grains is $\sigma^2 \times \sigma_1$ with $\sigma = 750$ nm and $\sigma_1 = 10.2$ μm the correlation lengths along the x/y and z direction. We characterize the strength of the disorder by the spatial average $\bar{V}$ of the speckle potential at the cloud position.

We create the rotated speckle pattern by transmitting a laser beam through two glass plates with random surface structures, i.e., diffusers, rotated against each other, and

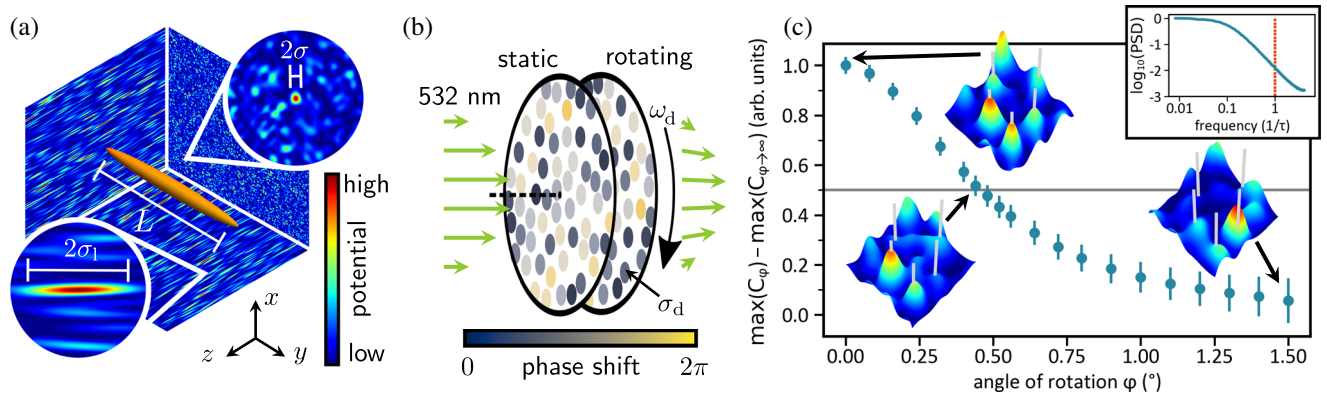

FIG. 1. (a) Sketch of experimental realization. Cigar-shaped clouds of $^6Li_2$ molecules with typical size $L \sim 300$ μm are exposed to an anisotropic speckle potential. (b) Creation of dynamic speckle. The dots with size σ_d represent the random surface of the diffusers, and their colors indicate the magnitude of the phase shift they imprint on incident light. The transmitted light is focused on the cloud. (c) Evolution of a dynamic speckle pattern. Maximum value of the cross-correlation function C_φ of the speckle intensity. Error bars mark the uncertainty of a fit that is used to extract the maximum value from C_φ. Insets: a section of a simulated speckle pattern with $\max(C_\varphi)$, as indicated by the arrows. Gray lines mark the positions of five distinct peaks in the initial speckle and simplify tracking the evolution of the intensity distribution. The inset plot shows the calculated temporal power spectral density (PSD) of a dynamic speckle (blue, solid line), where the inverse correlation time roughly coincides with the frequency at which PSD has dropped to $1/100$ of its maximum value at zero frequency. For comparison, we also show the PSD of a speckle whose mean potential is periodically modulated with frequency $1/\tau$ (red, dashed).

focusing the light field onto the atoms [Fig. 1(b)]. Upon rotation, the local phase imprints change significantly, causing the height and position of the interference pattern's speckle grains to change. We quantify the resemblance to the initial speckle intensity distribution $I_{\varphi=0^\circ}$ by the maximum value of the cross-correlation function [34], $\max(C_\varphi)$, with

$$C_\varphi(x,y) = \int dx'dy' I_{\varphi=0^\circ}(x',y') I_\varphi(x'+x, y'+y). \qquad (1)$$

$I_\varphi(x,y)$ are two-dimensional intensity distributions in the focal plane for rotation angle φ of the diffuser plate, independently measured in a test setup. We define the correlation angle φ_c at which $\max(C_\varphi)$ has dropped to half its initial value; see Fig. 1(c). For rotation at constant angular velocity ω_d, the correlation angle translates into a correlation time $\tau = \varphi_c/\omega_d$. In the experimental setup, $\omega_d \leq 2100\,^\circ\mathrm{s}^{-1}$ and $\varphi_c = 0.6^\circ$; hence $\tau > 285$ μs. Importantly, in contrast to a periodically driven potential, the temporal power-spectral density of this dynamic speckle comprises a broad distribution of frequencies, where low-frequency contributions dominate, and the inverse correlation time can be interpreted as a bandwidth or cutoff frequency [see inset of Fig. 1(c)].

To study the response of thermal clouds to the dynamic disorder, we prepare samples with 3.4×10^5 molecules with $a = 1524\,a_0$ (a_0 is the Bohr radius) in a trap with harmonic frequencies $\omega_x, \omega_y, \omega_z = 2\pi \times (498, 22.1, 340)$ Hz at a temperature of $T = 590$ nK. Following the end of the evaporation ramp, the cloud is allowed to relax for 500 ms to ensure thermal equilibrium. In order to minimize excitations in the gas, we increase the potential of the dynamic speckle during a 50 ms linear ramp to its final value of $\bar{V}/k_B = 30.5$ nK $\ll T$, where k_B is the Boltzmann constant. After a variable hold time $d_s \leq 180$ ms, the speckle is extinguished during 50 ms, and we take an absorption image of the trapped cloud. We extract the temperature by fitting a Bose-enhanced Gaussian function [35] to the integrated column-density distribution. We observe that the cloud temperature T is proportional to the hold time d_s and the slope, i.e., the heating rate $P = dT/dd_s$, grows with increasing $1/\tau$; see Fig. 2(a). The heating rate is extracted by fitting a linear function to the data. We compare these results to a numerical simulation of classical, non-interacting point particles with thermal velocity distribution in a dynamic, homogeneous speckle in two dimensions [36]. The dimensional reduction is facilitated by the anisotropic speckle, which allows one to neglect the much weaker potential gradients along the z axis as compared with the xy plane. The heating rates from this simulation [Fig. 2(b)] yield good agreement with the experimental data. We conclude that the heating is intrinsically a single-particle effect, not modified by the elastic molecule-molecule scattering at a rate of 11 ms^{-1} or inelastic collisions. Moreover, we develop a microscopic heating model based on a random walk in momentum space for the limiting case $k_BT \gg \bar{V}$, which is realized in the experiment. Single particles travel on almost straight trajectories, and experience "kicks" with momentum change $\Delta p \ll p$ from the time-dependent potential. The resulting heating rate is given by

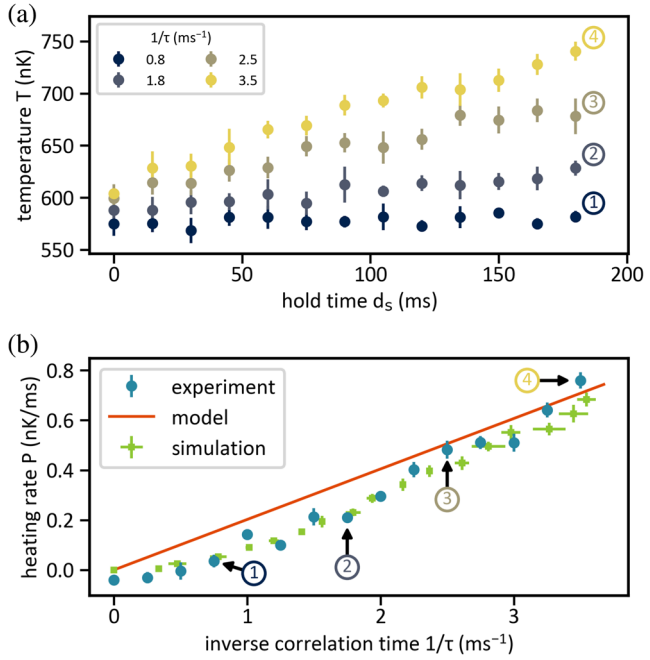

FIG. 2. Heating of a thermal ensemble with initial temperature $T = 590$ nK in dynamic speckle disorder with $\bar{V} = 30.5\ \mathrm{nK} \times k_B$. (a) Cloud temperature T versus hold time d_s for various values of $1/\tau$. (b) Heating rate P versus inverse correlation time $1/\tau$. Squares result from the numerical simulation, solid line from the microscopic model. Error bars of experimental data in (b) denote uncertainty of the fit, other errors the standard deviation of 5 repetitions.

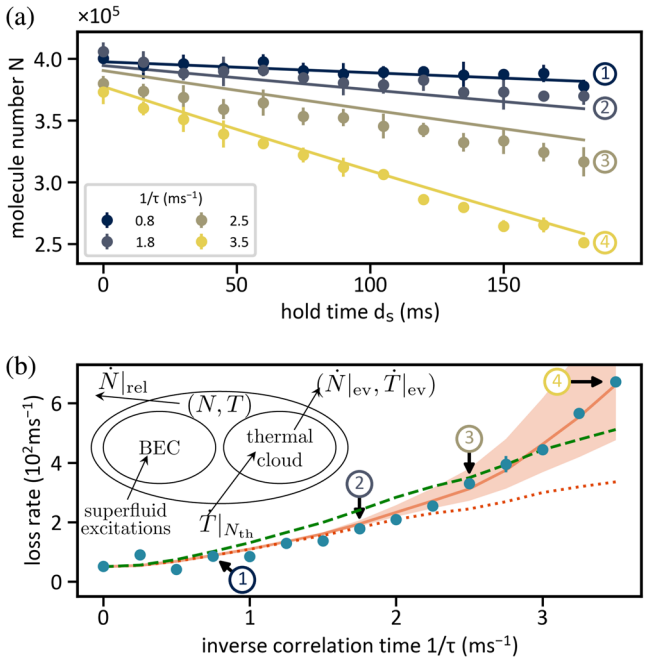

FIG. 3. Dissipation of a BEC in dynamic disorder. (a) Total molecule number N versus hold time d_s for various values of $1/\tau$. Error bars denote the standard deviation of 5 repetitions. Solid lines are from the rate model. (b) Loss rates versus inverse correlation time $1/\tau$. Error bars of experimental data points (blue) show the error estimation of the linear fit and are smaller than the marker size for most data points. Lines indicate results from the rate model, including thermal heating and phenomenologically superfluid excitations in the inhomogeneous gas (solid), thermal heating and microscopic particle loss from the homogeneous condensate (dashed green), or only heating of the thermal cloud (dotted). The shaded area represents a ±20% variation of v_s. Inset: the processes included in the open-system rate model.

$$P = \frac{\bar{V}^2}{2k_B^2 T\tau}\gamma, \tag{2}$$

where the constant γ corrects for the dimensionality and the trapping potential in each dataset independently [36]. The model matches the measured heating rates for sufficiently large inverse correlation times [Fig. 2(b)] [37].

In order to study quantum gases in dynamical disorder, we cool samples with $N = 4 \times 10^5$ molecules and scattering length $a = 2706\,a_0$ to $T = 50$ nK, far below the noninteracting critical temperature of condensation $T_c = 245$ nK. Hence, we expect a condensate fraction > 0.8 and a BEC with chemical potential $\mu = 250\ \mathrm{nK} \times k_B = 5.2\ \mathrm{kHz} \times h$, where h is Planck's constant. The corresponding timescale $h/\mu = 190\ \mu$s is smaller than the experimentally accessible correlation times, and the healing length at the trap center $\xi = 380$ nm [41] falls below the correlation lengths. Thus, for these maximum values, the condensate can temporally react to and spatially resolve all changes and details of the speckle potential. The experimental sequence for the exposure to the dynamic speckle is the same as for thermal clouds. Instead of the temperature, we monitor the total molecule number N of the sample, because the large condensed fraction does not allow one to extract a temperature from absorption images reliably. We find that the molecule number decreases linearly with d_s, and the loss rate $-dN/dd_s$ grows with $1/\tau$ (see Fig. 3). We distinguish two main processes contributing to the loss of molecules from the trap. On the one hand, as described before, the dynamic speckle heats the residual thermal component of the gas. The rising temperature causes molecules to transfer from the BEC to the thermal fraction, from which molecules with sufficient energy can evaporate, which in turn cools the sample. On the other hand, the motion of the dynamic speckle creates excitations in the BEC, which again diminishes the condensate fraction because of Landau damping [42]. We model the underlying dynamics by two approaches. The first takes into account the trap but treats superfluid damping in a phenomenological way, whereas the second provides analytic expressions for the particle loss from the condensate fraction in a homogeneous superfluid.

Due to the BEC being superfluid, excitations are mainly expected if the typical velocity v_s of the speckle exceeds the local Landau critical velocity $v_c(\boldsymbol{r}) = \sqrt{gn_0(\boldsymbol{r})/m}$ in the condensate, where n_0 is the condensate density distribution and g the coupling constant [41]. These local

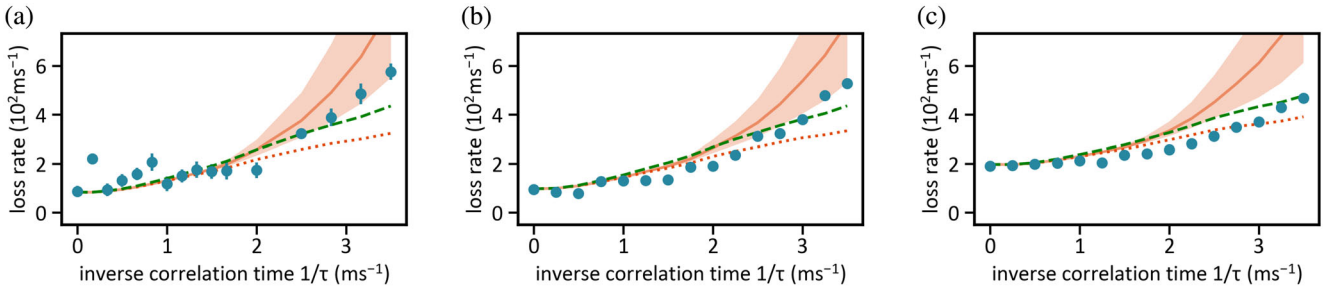

FIG. 4. Loss rates of BECs in dynamic speckle for various values of the s-wave scattering length a. The allocation of colors and line styles is the same as in Fig. 3(b). (a) $a = 1524a_0$, $\mu = 187$ nK $\times k_B = 3.9$ kHZ $\times h$; (b) $a = 1310a_0$, $\mu = 173$ nK $\times k_B = 3.6$ kHz $\times h$; (c) $a = 982a_0$, $\mu = 144$ nK $\times k_B = 3.0$ kHz $\times h$. The range of interaction strengths explored is limited for lower interactions by the decreasing collisional lifetime of molecules and for higher interactions by the emergence of free atoms as the binding energy decreases.

quantities are well defined because, for our parameters, the local-density approximation is valid [43]. We can estimate the largest velocity scale of the speckle from the correlation lengths and time to be $v_s = \sqrt[3]{\sigma^2\sigma_1}/\tau < 6.3$ mm s^{-1}, which is below the maximum critical velocity $v_c(\mathbf{0}) = 13.2$ mm s^{-1} at the center of the condensate. However, because of the Thomas-Fermi density profile [44], there are always regions with $v_c(\boldsymbol{r}) < v_s$ where excitations are possible. Additionally, inelastic collisions between molecules cause losses, even in the absence of any speckle potential [45]. We capture this interplay between heating, evaporation, and cooling by a set of rate equations

$$\dot{N} = \dot{N}|_{\mathrm{ev}} + \dot{N}|_{\mathrm{rel}} \tag{3}$$

$$\dot{T} = \dot{T}|_{N_{\mathrm{th}}} + \dot{T}|_{\mathrm{ev}} + (\dot{T}|_{N_0}) \tag{4}$$

modeling the open quantum system (for details see the Supplemental Material [36]), which includes the processes evaporation from the thermal component $(\dot{N}|_{\mathrm{ev}}, \dot{T}|_{\mathrm{ev}})$, molecular relaxation $\dot{N}|_{\mathrm{rel}}$, and heating of the thermal component by the dynamic speckle $\dot{T}|_{N_{\mathrm{th}}}$ [see inset of Fig. 3(b)]. We calculate the number of superfluid molecules $N_0 = N \times n_c(T/T_c, N, a)$ using an expression for the condensate fraction n_c, which incorporates the intermolecular interaction and finite size of the system [36,46]. We neglect effects of the relatively strong quantum depletion [46], because the depleted density remains superfluid [47]. The number of thermal molecules is given by $N_{\mathrm{th}} = N - N_0$ and we assume the system to be in thermal equilibrium at all times. In order to include the effect of the speckle potential onto the superfluid molecules, in a first approach, we calculate the fraction f of the ones located in regions of the condensate where $v_c(\boldsymbol{r}) < v_s$. We assume that in addition to thermally excited molecules N_{th}, the condensed particles in the former mentioned area $f \times N_0$ are removed from the system by evaporation. Numerically, we find that f is close to zero below $v_s/v_c(\mathbf{0}) = 0.3$ [36], which roughly coincides with $1/\tau \approx 2$ ms^{-1}. This model phenomenologically including superfluid excitations in the inhomogeneous system is indicated as solid line in Figs. 3 and 4.

This approach obviously neglects the intricate dynamics, interactions, and spectrum of superfluid excitations [48]. Therefore, in a second approach, we compute the rate of particles transferred from the condensate to the thermal fraction using number-conserving Bogoliubov theory in a speckle with Gaussian-shaped spatiotemporal spectrum [36,49], contributing another heating term $\dot{T}|_{N_0}$ in Eq. (4). For a homogeneous condensate, we find [36]

$$\dot{T}|_{N_0} = \frac{\eta^2 \bar{V}^2 T_c^3 \pi \sigma^3}{6T^2\hbar^2 v_c \xi \sqrt{\sigma^2 + v_c^2\tilde{\tau}^2}} e^u \{2u[I_{5/4}(u) - I_{3/4}(u) + I_{1/4}(u) - I_{-1/4}(u)] + I_{1/4}(u)\}, \tag{5}$$

where $I_\nu(u)$ are an modified Bessel function of the first kind [50], u is defined as $u = (\sigma^2 + v_c^2\tilde{\tau}^2)^2/16\xi^2 v_c^2\tilde{\tau}^2$, and $\tilde{\tau} = \tau/\sqrt{\log 2}$. In order to adopt the homogeneous theory to the inhomogeneous experimental system, we use the parameter η, which we set to $\eta \approx 0.05$, effectively accounting for the experimental speckle anisotropy and effects of the speckle's inhomogeneity to roughly yield the experimental particle loss rate [36], and evaluate Eq. (5) with the mean superfluid density. This value of η has been obtained by calculating the loss rates for all experimental parameter sets and for several values of η. We solve Eqs. (3) and (4) numerically to obtain the time dependence of the particle number and compare the results to the experimental data in Fig. 3, where this model microscopically including particle loss in a homogeneous system is shown as a dashed line. Both models reproduce the measured loss rates closely. Molecular relaxation is included via the relaxation rate α such that the loss rate in the static speckle matches the measured one; we find agreement with previously reported values [36,51,52]. For relatively long correlation times $1/\tau \lesssim 2$ ms^{-1}, the losses due to superfluid excitations are negligible, and the loss rates are well captured merely by the heating of the thermal cloud [dotted line in Fig. 3(b)]. In the case of $1/\tau \gtrsim 2$ ms^{-1}, both loss mechanisms contribute significantly. Reducing the interaction strength, the

phenomenological rate model systematically overestimates the loss rate by assuming immediate depletion of condensate atoms in the region $v_c(\vec{r}) < v_s$ (see Fig. 4 and the Supplemental Material [36]), while the model computing the excitation rate from the condensate yields good agreement for all interaction strengths with one common fit parameter.

Our studies indicate a regime, where quantum fluids are shielded from direct superfluid excitations even for a broadband excitation, prevailing for a broad range of interaction strengths. The tight control over correlation times points toward future studies of transport in time-dependent disorder both for classical and quantum systems with strong interactions.

We thank Hans Kroha and Axel Pelster for fruitful discussions and Maximilian Kaiser for carefully reading the manuscript. This work was supported by the Deutsche Forschungsgemeinschaft (DFG, German Research Foundation) via the Collaborative Research Center SFB/TR185 (Project No. 277625399). J. K. and M. W. were supported by the Max Planck Graduate Center with the Johannes Gutenberg-Universität Mainz (MPGC).

*widera@physik.uni-kl.de

[1] T. Vojta, Disorder in quantum many-body systems, Annu. Rev. Condens. Matter Phys. **10**, 233 (2019).
[2] *50 Years of Anderson Localization*, edited by E. Abrahams (World Scientific, Singapore; London, 2010).
[3] P. W. Anderson, Absence of diffusion in certain random lattices, Phys. Rev. **109**, 1492 (1958).
[4] D. S. Wiersma, P. Bartolini, A. Lagendijk, and R. Righini, Localization of light in a disordered medium, Nature (London) **390**, 671 (1997).
[5] G. Roati, C. D'Errico, L. Fallani, M. Fattori, C. Fort, M. Zaccanti, G. Modugno, M. Modugno, and M. Inguscio, Anderson localization of a non-interacting Bose–Einstein condensate, Nature (London) **453**, 895 (2008).
[6] J. Billy, V. Josse, Z. Zuo, A. Bernard, B. Hambrecht, P. Lugan, D. Clément, L. Sanchez-Palencia, P. Bouyer, and A. Aspect, Direct observation of Anderson localization of matter waves in a controlled disorder, Nature (London) **453**, 891 (2008).
[7] S. S. Kondov, W. R. McGehee, W. Xu, and B. DeMarco, Disorder-Induced Localization in a Strongly Correlated Atomic Hubbard Gas, Phys. Rev. Lett. **114**, 083002 (2015).
[8] M. Schreiber, S. S. Hodgman, P. Bordia, H. P. Luschen, M. H. Fischer, R. Vosk, E. Altman, U. Schneider, and I. Bloch, Observation of many-body localization of interacting fermions in a quasirandom optical lattice, Science **349**, 842 (2015).
[9] J. Z. Imbrie, On many-body localization for quantum spin chains, J. Stat. Phys. **163**, 998 (2016).
[10] J. Smith, A. Lee, P. Richerme, B. Neyenhuis, P. W. Hess, P. Hauke, M. Heyl, D. A. Huse, and C. Monroe, Many-body localization in a quantum simulator with programmable random disorder, Nat. Phys. **12**, 907 (2016).
[11] K. X. Wei, C. Ramanathan, and P. Cappellaro, Exploring Localization in Nuclear Spin Chains, Phys. Rev. Lett. **120**, 070501 (2018).
[12] P. Hänggi and F. Marchesoni, Artificial Brownian motors: Controlling transport on the nanoscale, Rev. Mod. Phys. **81**, 387 (2009).
[13] S. Gopalakrishnan, K. R. Islam, and M. Knap, Noise-Induced Subdiffusion in Strongly Localized Quantum Systems, Phys. Rev. Lett. **119**, 046601 (2017).
[14] A. M. Jayannavar and N. Kumar, Nondiffusive Quantum Transport in a Dynamically Disordered Medium, Phys. Rev. Lett. **48**, 553 (1982).
[15] L. Levi, Y. Krivolapov, S. Fishman, and M. Segev, Hyper-transport of light and stochastic acceleration by evolving disorder, Nat. Phys. **8**, 912 (2012).
[16] P. Rebentrost, M. Mohseni, I. Kassal, S. Lloyd, and A. Aspuru-Guzik, Environment-assisted quantum transport, New J. Phys. **11**, 033003 (2009).
[17] A. W. Chin, A. Datta, F. Caruso, S. F. Huelga, and M. B. Plenio, Noise-assisted energy transfer in quantum networks and light-harvesting complexes, New J. Phys. **12**, 065002 (2010).
[18] M. A. Ratner and A. Nitzan, Conductivity in polymer ionics. Dynamic disorder and correlation, Faraday Discuss. **88**, 19 (1989).
[19] G. S. Grest, I. Webman, S. A. Safran, and A. L. R. Bug, Dynamic percolation in microemulsions, Phys. Rev. A **33**, 2842 (1986).
[20] I. Sendiña-Nadal, S. Alonso, V. Pérez-Muñuzuri, M. Gómez-Gesteira, V. Pérez-Villar, L. Ramírez-Piscina, J. Casademunt, J. M. Sancho, and F. Sagués, Brownian Motion of Spiral Waves Driven by Spatiotemporal Structured Noise, Phys. Rev. Lett. **84**, 2734 (2000).
[21] A. L. Virovlyansky, D. V. Makarov, and S. V. Prants, Ray and wave chaos in underwater acoustic waveguides, Phys. Usp. **55**, 18 (2012).
[22] A. G. Aronov and P. Wölfle, Effect of a fluctuating magnetic field on weak localization in a two-dimensional disordered system, Phys. Rev. B **50**, 16574 (1994).
[23] Y. Yin, D. E. Katsanos, and S. N. Evangelou, Quantum walks on a random environment, Phys. Rev. A **77**, 022302 (2008).
[24] C. Van den Broeck, J. M. R. Parrondo, and R. Toral, Noise-Induced Nonequilibrium Phase Transition, Phys. Rev. Lett. **73**, 3395 (1994).
[25] J. García-Ojalvo and J. M. Sancho, Colored noise in spatially extended systems, Phys. Rev. E **49**, 2769 (1994).
[26] A. Eckardt, Colloquium: Atomic quantum gases in periodically driven optical lattices, Rev. Mod. Phys. **89**, 011004 (2017).
[27] K. Singh, C. J. Fujiwara, Z. A. Geiger, E. Q. Simmons, M. Lipatov, A. Cao, P. Dotti, S. V. Rajagopal, R. Senaratne, T. Shimasaki, M. Heyl, A. Eckardt, and D. M. Weld, Quantifying and Controlling Prethermal Nonergodicity in Interacting Floquet Matter, Phys. Rev. X **9**, 041021 (2019).
[28] H.-P. Breuer and F. Petruccione, *The Theory of Open Quantum Systems* (Oxford University Press, New York, 2007).
[29] F. T. Arecchi, Measurement of the Statistical Distribution of Gaussian and Laser Sources, Phys. Rev. Lett. **15**, 912 (1965).
[30] B. Gänger, J. Phieler, B. Nagler, and A. Widera, A versatile apparatus for fermionic lithium quantum gases based on an

interference-filter laser system, Rev. Sci. Instrum. **89**, 093105 (2018).
[31] B. Nagler, M. Radonjić, S. Barbosa, J. Koch, A. Pelster, and A. Widera, Cloud shape of a molecular Bose–Einstein condensate in a disordered trap: A case study of the dirty boson problem, New J. Phys. **22**, 033021 (2020).
[32] G. Zürn, T. Lompe, A. N. Wenz, S. Jochim, P. S. Julienne, and J. M. Hutson, Precise Characterization of ^{6}Li Feshbach Resonances Using Trap-Sideband-Resolved RF Spectroscopy of Weakly Bound Molecules, Phys. Rev. Lett. **110**, 135301 (2013).
[33] J. W. Goodman, *Speckle Phenomena in Optics* (Roberts and Company Publishers, 2007).
[34] A. Papoulis and McGraw-Hill, *The Fourier Integral and Its Applications*, Classic Textbook Reissue Series (McGraw-Hill, New York, 1962).
[35] W. Ketterle, D. Durfee, and D. Stamper-Kurn, Making, probing and understanding Bose-Einstein condensates, in *Proceedings of the International School of Physics "Enrico Fermi"*, edited by M. Inguscio, S. Stringari, and C. E. Wieman (1999), Vol. 140, pp. 61–176.
[36] See Supplemental Material at http://link.aps.org/supplemental/10.1103/PhysRevLett.128.233601 for details of the experimental setup and of the numerical and analytical models used.
[37] For the complementary regime of high particle velocities, theoretical works on the transport of classical particles in dynamic disorder predict a universal time dependence of the average kinetic energy of a particle $E_{\mathrm{kin}} \propto t^{2/5}$ [38–40]. Numerical simulations of our system reproduce power-law behavior with different exponents for sufficiently long observation times.
[38] L. Golubović, S. Feng, and F.-A. Zeng, Classical and Quantum Superdiffusion in a Time-Dependent Random Potential, Phys. Rev. Lett. **67**, 2115 (1991).
[39] M. N. Rosenbluth, Comment on "Classical and Quantum Superdiffusion in a Time-Dependent Random Potential", Phys. Rev. Lett. **69**, 1831 (1992).
[40] Y. Krivolapov and S. Fishman, Universality classes of transport in time-dependent random potentials, Phys. Rev. E **86**, 030103(R) (2012).
[41] C. J. Pethick and H. Smith, *Bose–Einstein Condensation in Dilute Gases*, 2nd ed. (Cambridge University Press, Cambridge, England, 2008).
[42] L. Pitaevskii and S. Stringari, Landau damping in dilute Bose gases, Phys. Lett. A **235**, 398 (1997).
[43] Y. Kagan, G. V. Shlyapnikov, and J. T. M. Walraven, Bose-Einstein Condensation in Trapped Atomic Gases, Phys. Rev. Lett. **76**, 2670 (1996).
[44] L. Pitaevskii and S. Stringari, *Bose–Einstein Condensation and Superfluidity*, International Series of Monographs on Physics (Oxford University Press, New York, 2016).
[45] D. S. Petrov, C. Salomon, and G. V. Shlyapnikov, Weakly Bound Dimers of Fermionic Atoms, Phys. Rev. Lett. **93**, 090404 (2004).
[46] H. Xiong, S. Liu, G. Huang, Z. Xu, and C. Zhang, Critical temperature and condensate fraction of the trapped interacting Bose gas with finite-size effects, J. Phys. B **34**, 3013 (2001).
[47] A. Miller, D. Pines, and P. Nozières, Elementary excitations in liquid helium, Phys. Rev. **127**, 1452 (1962).
[48] A. J. Leggett, *Quantum Liquids: Bose Condensation and Cooper Pairing in Condensed-Matter Systems* (Oxford University Press, United States, 2008).
[49] Y. Castin, Bose-einstein condensates in atomic gases: Simple theoretical results, in *Coherent Atomic Matter Waves*, edited by R. Kaiser, C. Westbrook, and F. David (Springer Berlin Heidelberg, Berlin, Heidelberg, 2001), pp. 1–136.
[50] M. Abramowitz and I. A. Stegun, *Handbook of Mathematical Functions with Formulas, Graphs, and Mathematical Tables*, 9th dover printing, 10th gpo printing ed. (Dover, New York, 1964).
[51] J. Cubizolles, T. Bourdel, S. J. J. M. F. Kokkelmans, G. V. Shlyapnikov, and C. Salomon, Production of Long-Lived Ultracold Li_2 Molecules from a Fermi Gas, Phys. Rev. Lett. **91**, 240401 (2003).
[52] S. Jochim, M. Bartenstein, A. Altmeyer, G. Hendl, C. Chin, J. H. Denschlag, and R. Grimm, Pure Gas of Optically Trapped Molecules Created from Fermionic Atoms, Phys. Rev. Lett. **91**, 240402 (2003).